NUREG/CR-1376
SAND80-0717

RISK METHODOLOGY FOR GEOLOGIC DISPOSAL OF RADIOACTIVE WASTE: THE DISTRIBUTED VELOCITY METHOD OF SOLVING THE CONVECTIVE-DISPERSION EQUATION

James E. Campbell and Dennis E. Longsine
Sandia National Laboratories
Albuquerque, New Mexico 87185

and

Mark Reeves
INTERA Environmental Consultants, Inc.
Houston, Texas 77079

Date Published: June 1980

Sandia National Laboratories
Albuquerque, New Mexico 87185
operated by
Sandia Corporation
U.S. Department of Energy

Prepared for
Office of Nuclear Regulatory Research
Probabilistic Analysis Staff
U.S. Nuclear Regulatory Commission
Washington, DC 20555
Under Memorandum of Understanding DOE 40-550-75
NRC FIN No. A-1192

ABSTRACT

A new method is proposed for treating convective-dispersive transport. The motivation for developing this technique arises from the demands of performing a risk assessment for a nuclear waste repository. These demands include computational efficiency over a relatively large range of Peclet numbers and the ability to handle chains of decaying radionuclides with rather extreme contrasts in both solution velocities and half lives. To the extent it has been tested to date, the Distributed Velocity Method (DVM) appears to satisfy these demands. Included in this paper are the mathematical theory, numerical implementation, an error analysis employing statistical sampling and regression analysis techniques, and comparisons of DVM with other methods for convective-dispersive transport.

TABLE OF CONTENTS

ACKNOWLEDGMENTS

The authors gratefully acknowledge Ron Iman of Sandia National Laboratories for his assistance in performing the error analysis presented in this report. Ron Lantz and Ed Tang of INTERA Environmental Consultants, Inc., are also acknowledged for their many helpful suggestions.

CHAPTER I. INTRODUCTION

The motivation for this work arises in the context of a risk analysis methodology for nuclear waste repositories (Campbell, et al., 1978). In such analysis, results are calculated using mathematical models which describe a number of processes. One of these processes is radionuclide migration in groundwater from the depository to a discharge point to the surface environment. Risk analysis necessarily involves large numbers of calculations. Furthermore, radionuclide migration times from the depository to the surface environment are typically long so that radionuclides in the actinide chains are likely to be significant contributors to risk. Thus a radionuclide transport model for use in risk assessment must be computationally efficient and must provide the ability to model transport of chains of radionuclides.

There are two general classes of techniques which may be used to simulate the migration of miscible trace constituents within a convecting medium. The first class solves the appropriate partial differential equations. The finite-difference method (Ames, 1977) and the finite-element method (Pinder and Gray, 1977), with, perhaps, special modifications for convection-dominant transport, are examples of this first class of techniques. The second class directly simulates the migration of representative particles of the trace constituent. One example of this second class of techniques is the Method of Characteristics (Garder, Peaceman

and Pozzi, 1963). Another example is the Monte Carlo method (Ahlstrom, et al, 1977).

In terms of the requirements of a risk methodology, each of the above techniques appears to have a problem. The various finite-difference and finite-element schemes have several criteria which limit the space and time steps Δx and Δt. These criteria may be expressed in terms of the Peclet number p, the Courant number c, and combinations thereof. These dimensionless numbers are defined by

$$p = \frac{\Delta x}{\alpha} \quad \text{and} \quad c = \frac{v\Delta t}{\Delta x} \tag{1-1}$$

where v is the interstitial velocity and α is the dispersivity (all symbols are defined in the section on nomenclature). For example, a standard finite-difference scheme, which is centered in space and time, requires that

$$p \leq 2 \quad \text{and} \quad c \cdot \left(1 + \frac{2}{p}\right) \leq 2 \tag{1-2}$$

to prevent overshoot (Price, Varga and Warren, 1966; Tang, 1980a; and Noble, 1969). Although criteria such as Eq. (1-2) have not been derived for the finite-element method, practical experience indicates that they are similar to those of Eq. (1-2) for centered-in-time differencing. Thus for applications involving large numbers of calculations with realistic but relatively small values of α, the finite-difference and finite-element methods

may be prohibitively expensive because of the required fineness of the space and time mesh.

The direct-simulation approaches which have been used in the past have difficulty in treating radioactive decay chains in which the different species have differing retardations. Presumably a set of particles would be required for each species, which would, in many cases, lead to excessive computer storage.

The technique presented in this report, the Distributed Velocity Method (DVM), is a direct simulation approach. It is quite similar to the Phase-Space-Time-Evolution (PSTE) Method for neutron transport (Jones and Campbell, 1978). In DVM, as in PSTE, tracking of individual particles is avoided by treating an ensemble of particles. In the numerical implementation of DVM (Chapter III), the spatial extent of an ensemble of particles is taken to be one grid block. This grid block averaging introduces numerical dispersion which is examined in Chapter IV using statistical sampling and regression techniques. Finally, Chapter V shows comparisons between DVM results and results obtained from other techniques.

In this, our initial investigation of DVM, we use a one-dimensional, constant velocity system which is the usual procedure for establishing error criteria. Furthermore, the resulting model is directly applicable in risk assessment for nuclear waste repositories. To qualify for more general site

analyses, however, the method must be extended to variable-velocity and multi-dimensional systems. Such extensions will be examined in future work.

CHAPTER II. THEORY

The objective of this section is to show basic concepts. Consequently, a single species is considered to be transported in one dimension via the mechanisms of convection and dispersion. Radioactive chains and sorption are not difficult to treat, but their inclusion tends to obscure the simplicity of the Distributed Velocity Method (DVM). Although decay chains and sorption are not considered in this chapter, they are included in numerical implementation in the next chapter. Multiple dimensions are not considered in this report.

Direct Simulation with DVM. The thinking underlying DVM is as follows: Consider a receiver point located at x and donor points located at some typical coordinate x'. Taking the density of an ensemble of particles at x' to be $\rho(x', t')$, the density $\rho(x, t)$ at x for $t > t'$ may be determined by introducing a velocity distribution.

The concept here is that, due to heterogeneity of the flow field, (Schwartz, 1977 and Tang, 1980b) a number of alternate paths exist for migration of particles from x' to x. Such paths may be characterized by a continuum of migration times and average velocity components v in the direction of flow. The distribution of such velocities is P(v). Thus for the donor point x', only those particles with average velocity $v = (x-x')/(t-t')$ arrive at point x at time t'. The density

of particles at point x may therefore be obtained by summing over all possible donor points in the following manner:

$$\rho_o(x,t) = \int_{-\infty}^{\infty} dv\ P(v)\ \rho(x-v\Delta t,\ t-\Delta t) \qquad (2\text{-}1)$$

where

$$\Delta t = t - t'$$

For convenience, P(v) is represented as a function of velocity only. However, it is certainly possible for P to be a function of other variables such as position x or time increment Δt. Otherwise, the functional form of the distribution is completely general at this point. In the next section, P(v) is specialized to a gaussian form which is appropriate for a conventional treatment of dispersion.

Eq. (2-1) gives the propagation of the initial conditions, at time t', to time t. If, in addition, a source $S(x', \tau)$ is included, then an integration over "injection" time must be performed in addition to an integration over velocity:

$$\rho(x,t) = \rho_o(x,t] + \int_{t'}^{t} d\tau \int_{v_1}^{v_o} dv\ P(v)\ S(x',\tau) \qquad (2\text{-}3)$$

where $x' = x - v(t-\tau)$. If $S(x',\tau)$ is nonzero only for (2-4)

$$x_o \leq x' \leq x_1 \qquad (2\text{-}5)$$

then the velocity limits for the source term of Eq. (2-3) are

$$v_o = (x - x_o)/(t - \tau) \tag{2-6}$$

and

$$v_1 = (x - x_1)/(t - \tau) \ . \tag{2-7}$$

Sources may arise either by leaching of the radioactive wastes in the depository or by decay of a radioactive parent. For the former, the spatial limits, and hence the velocity limits, are determined by the location of the depository as indicated above. For the latter, the spatial location of the source (i.e., the radioactive parent) is time dependent.

Connection with Green's Function. The inhomogeneous convective dispersion equation in one dimension can be written as

$$\frac{\partial \rho}{\partial t} = D \frac{\partial^2 \rho}{\partial x^2} - \bar{v} \frac{\partial \rho}{\partial x} + S \tag{2-8}$$

for null conditions on ρ at the infinite boundaries, the solution to Eq. (2-8) contains two terms. One is the complementary solution

$$\rho_o(x,t) = \int_{-\infty}^{\infty} dx' \ \rho(x',t') \ G(x-x', \ t-t') \tag{2-9}$$

The other term is a particular solution of Eq. (2-8) which yields the complete solution

$$\rho(x,t) = \rho_o(x,t) + \int_{t'}^{t} d\tau \int_{x_o}^{x} dx' \; S(x',\tau) \; G(x-x',\, t-t') \qquad (2\text{-}10)$$

The Green's function of Eqs. (2-9) and (2-10) may be written

$$G(x-x',\, t-t') = \frac{1}{\sqrt{2\pi}\,\sigma_x} \exp - \left(\frac{[(x-x') - v(t-t')]^2}{2\,\sigma_x^2} \right) \qquad (2\text{-}11)$$

where the variance is

$$\sigma_x^2 = 2D(t - t') \qquad (2\text{-}12)$$

Here G is a spatial Green's function, as indicated by the units of σ_x (i.e., length) and G (i.e., 1/length).

Eq. (2-11) may be recast as a velocity distribution by considering Figure 1. This figure illustrates the evolution of G over t - t' from a Dirac delta function to a gaussian distribution. Particles arriving at the mean position of this spatial distribution have travelled from x' with velocity $\bar{v}$. Particles at position x, however, have travelled from x' with an average velocity

$$v = (x - x')/(t - t') \qquad (2\text{-}13)$$

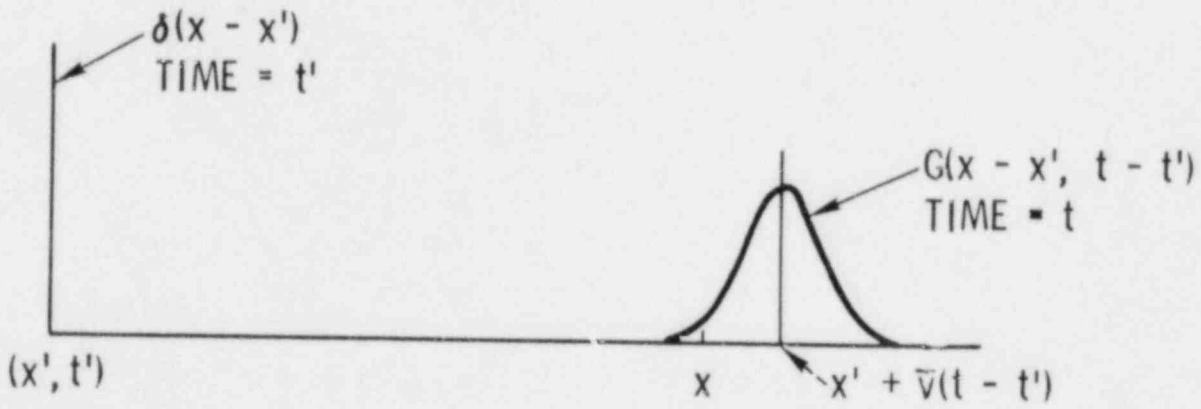

Figure 1. The Spatial Green's Function

If Eq. (2-13) is substituted into Eqs. (2-11) and (2-12), then

$$G(x-x',\ t-t') = G(v,\ t-t')/(t-t') \tag{2-14}$$

where

$$G(v,\ t-t') = \frac{1}{\sqrt{2\pi}\ \sigma_v} \exp\left\{-\frac{(v-\bar{v})}{2\ \sigma_v^2}\right\}^2 \tag{2-15}$$

and

$$\sigma_v = \sqrt{2D/(t-t')} = \sigma_x/(t-t') \tag{2-16}$$

Quantity G is a Green's function in velocity space as indicated by the units of σ_v, i.e., (length/time) and G, i.e., (length/time)$^{-1}$.

If Eq. (2-14) is substituted into Eqs. (2-9) and (2-10), Eqs. (2-2) and (2-3) are recovered with the velocity distribution P(v) identified as the gaussian form of Eq. (2-15).

CHAPTER III. NUMERICAL IMPLEMENTATION

The purposes of this chapter are threefold, namely (1) to numerically implement the integral equations of Chapter II, (2) to generalize the treatment to include sorption and radioactive decay chains and (3) to discuss source and sink models. In the first section only one decaying species is considered. In the second section, the analysis is extended to the treatment of a radioactive decay chain. In the last section a source model, which includes both leach and solubility limitations, and a discharge model are presented.

One Decaying Radionuclide. Here we consider only the propagation of the density function $\rho(x', t')$ from time t' to time t (c. f. Eq. 2-1). Initially, the space-velocity domain is discretized as in Figure 2. There are N_x equal space increments Δx and the time increment Δt is taken to be a constant. The velocity dimension is divided into N_v increments based on equal probability. The implementation of DVM can be generalized to variable spatial and time increments but such generalization is not considered in this report.

Propagation of densities over time-step Δt for velocity subgroup j may be written

$$\Delta\rho(i,j,t) = DW(j) \left\{ M(j)\ \rho(i-k_j,\ t') + [1-M(j)]\ \rho(i-k_j-1,\ t') \right\} \tag{3-1}$$

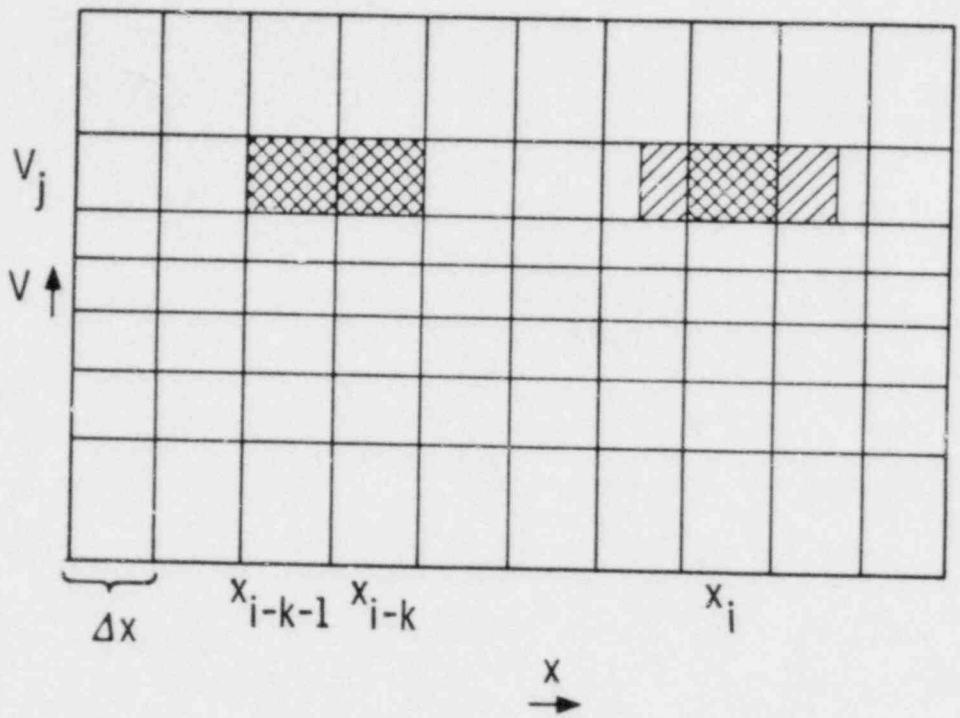

Figure 2. Discretized Velocity - Space Domain

Although the argument list in Eq. (3-1) appears formidable, it can be readily understood. As indicated there, the contribution to receiver block i for velocity interval j is determined by three fractions: a mixing fraction M, a velocity-interval fraction $\mathcal{W}$, and a decay fraction D.

The mixing fraction M may be understood by reference to Figure 2. Looking at velocity interval j, we see that there are, in general, two contributions to receiver block i. One is a packet of particles coming from donor block i - k and the other is a packet of particles from donor block i - k - 1. As is also indicated in Figure 2, there is generally only partial overlap of the propagated block contents with receiver block i. The donor block index k is

$$k_j = [[v_j \Delta t/\Delta x]] \tag{3-2}$$

where

$$[[x]] = \text{greatest integer} \leq x$$

and v_j is determined from

$$(j - \tfrac{1}{2})/N_v = \frac{1}{\sqrt{2\pi}\,\sigma_v} \int_{-\infty}^{v_j} \exp\left[\frac{-(v-\bar{v})^2}{2\,\sigma_v^2}\right] dv \,. \tag{3-3}$$

The corresponding mixing fraction is

$$M(j) = 1\ (v_j \Delta t/\Delta x - k_j)\ . \tag{3-4}$$

As the velocity dimension is divided into intervals based on equal probability, the weight $W(j)$ assigned the j_{th} velocity interval is just

$$W(j) = 1/N_v. \tag{3-5}$$

The decay fraction is taken to be

$$\mathcal{D} = e^{-\lambda t} \tag{3-6}$$

With these three fractions defined, Equation (3-1) is summed over all velocity intervals to obtain the total particle density in grid block i:

$$\rho(i,t) = \mathcal{D}/N_v \sum_{j=1}^{N_v} \Big\{ M(j)\ \rho(i - k_j,\ t') + \Big[1 - M(j)\Big]\ \rho(i - k_j - 1,\ t') \Big\}\ . \tag{3-7}$$

As a last step in this analysis, we express Equation (3-7) in a more computationally efficient manner. To do this, we note the possibility of degeneracy with respect to the index k_j. This could mean either

$$k_{j+1} = k_j \text{ or } k_{j+1} = k_j - 1 \tag{3-8}$$

Taking such degeneracies into account yields the expression

$$\rho(i,t) = \sum_{j=1}^{N_B(i)} B(j)\ \rho\ (i - k_j,\ t') \quad . \tag{3-9}$$

Quantities $N_B(i)$ and $B(j)$ are most easily obtained by a computational procedure which makes the tests of Eq. (3-8) and accumulates the coefficients to form the B matrix.

It is important to note that, so long as Δx and Δt are constants, B is a simple vector which contains at most $2 \cdot N_v$ terms. Furthermore, B(j) may be computed during the initial setup. For unequal grid block increments Δx, B would be dependent on grid block index i, and for unequal time increments Δt, B would have to be reevaluated for each change in time increment.

A Chain of Radionuclides. Here the starting point is similar to Eq. (3-1), and for species r of a radioactive decay chain it may be written as follows:

$$\Delta\rho(i,j,r,r-p,t) = \mathcal{D}(r,r-p)\mathcal{W}(j)\ \Big\{M(j,r,r-p) \cdot \rho(i-k_j,r-p,t') + [1-M(j,r,r-p)]\rho(i-k_j-1,r-p,t')\Big\} \tag{3-10}$$

In this equation $\Delta\rho$ is the incremental particle density for isotope r, grid block i, velocity subgroup j, and time t which arises from decay of isotope r - p. If p = 0, Eq. (3-10) degenerates to Eq. (3-1).

Quantity M, the mixing fraction, is determined by Eqs. (3-2) and (3-4) as before. The only difference here is the velocity. Because of sorption effects, the velocity will, in general, change with species during the decay $r - p \rightarrow r - p + 1 \rightarrow \ldots \rightarrow r$, which occurs during time step Δt. Hence, in this case, the velocity $\bar{v}(j, r, r-p)$ represents a species average. The velocity model currently being used is based on an equal partitioning of the time increment among the various species. This yields

$$\bar{v}(j,r,r-p) = \sum_{q=0}^{p} v(j,r-q)/(p + 1) \qquad (3\text{-}11)$$

In writing Eq. (3-11), it is assumed that the velocity subgroup does not change during radioactive decay over time step Δt. Weight W, the velocity subgroup fraction, is taken from Eq. (3-5) as before.

The role of quantity D in Eq. (3-10) is expanded beyond that of Eq. (3-1). In Eq. (3-1), D denotes that fraction which survives decay during Δt. In Eq. (3-10), D pertains to decay only when $p = 0$, i.e.,

$$D(r,r-p) = e^{-\lambda_r \Delta t}, \quad p = 0 \qquad (3\text{-}12)$$

Otherwise, this quantity denotes production of species r from species r - p, and may be developed from the Bateman equations

$$\mathcal{D}(r,\ r\text{-}p) = \prod_{q=1}^{p} \lambda_{r-q} \left\{ \sum_{i=1}^{p} \frac{e^{-\lambda_{r-i}\Delta t} - e^{-\lambda_{r}\Delta t}}{\prod_{\substack{j=o \\ j\neq i}}^{p} (\lambda_{r-j} - \lambda_{r-i})} \right\}, \quad p \neq o \qquad (3\text{-}13)$$

This equation, when coupled with appropriate mixing and weighting functions, may be viewed as a model for evaluating that portion of the source integral in Eq. (2-3) which is appropriate for radioactive decay processes. The accuracy of this model is demonstrated in Chapter V by two example calculations for three member chains and by comparison with analytic results.

To complete the analysis of radioactive decay chains, we need to sum Eq. (3-10) over all velocity subgroups j and all parents p of species r. This procedure yields

$$\rho(i,r,t) = \sum_{p=o}^{N_p(r)} \sum_{j=1}^{N_v} \mathcal{D}(r,\ r\text{-}p)\ W(j) \Big\{ M(j,\ r,\ r\text{-}p) \qquad (3\text{-}14)$$

$$\cdot \rho(i\text{-}k_j,\ r\text{-}p,\ t') + [1 - M(j,\ r,\ r\text{-}p)] \cdot \rho(i\text{-}k_j - 1,\ r\text{-}p,\ t') \Big\}$$

Recollecting the sum then gives the working equation

$$\rho(i,r,t) = \sum_{p=o}^{N_p(r)} \sum_{j=1}^{N_B(i,r,r-p)} B(j,\ r,\ r-p)\,\rho(i-k_j,\ r-p,\ t') \quad (3\text{-}15)$$

The upper bounds in Eq. (3-15) are expressed as functions. The dependence $N_p(i)$ reflects the fact that, in general, each nuclide has a different number of parents. Furthermore, one may want to arbitrarily impose a bound on the parent sum. The limit $N_B(i,\ r,\ r-p)$ gives the number of grid blocks which contribute to a receiver block i. It carries nuclide indices because of the velocity model [Eq. (3-11)]. As in the case of a single decaying nuclide, B will not vary with grid block or time step indices provided that Δx and Δt do not vary. Thus the B matrix may be generated during the setup process. As indicated in Eq. (3-15) B is a three-dimensional array. Its maximum dimension is typically less than 10 so that it may be easily stored. It should be noted, for purposes of comparison with other numerical techniques, that Equation (3-15) is an explicit relation in that each term on the right-hand side is known prior to solution for the unknown density $\rho(i,r,t)$.

Source and Discharge Models. For the present application of DVM, the source of radionuclides is considered to be a nuclear waste depository whose containment has been breached. To simulate such a source, the numerical implementation simply injects

radionuclides into an appropriate number of source grid blocks. A one-dimensional system with source blocks at the left side is shown in Figure 3. Discharge occurs when radionuclides pass the right boundary of the system.

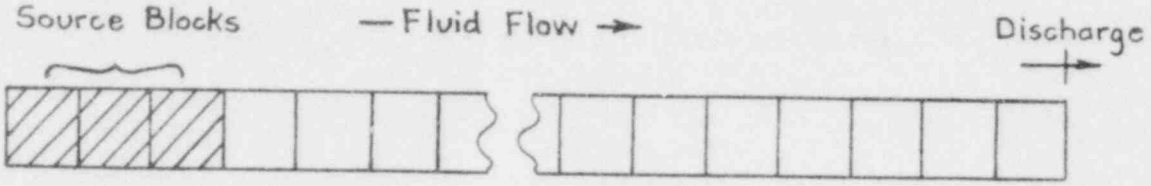

Figure 3. One Dimensional Flow System Showing Source Blocks and Discharge.

The source model accounts for both leach and solubility limits by considering three different radionuclide inventories; namely, (1) unleached, (2) leached but undissolved and and (3) dissolved. In the present version of DVM, the leach rate is assumed constant. However, generalization to a time-dependent leach rate is straightforward.

For a constant leach-rate model, the quantity of waste matrix leached during time step Δt is

$$\Delta m = \frac{m_o}{\tau} \Delta t \qquad (3\text{-}16)$$

where m_o is the initial mass of waste matrix and τ is the leach time. The concentration $N(r, t + \Delta t/2)$ of species r in the waste matrix at time $t + \Delta t/2$ is determined from

$$N(r, t+\Delta t/2) = \sum_{p=o}^{N_p(r)} \mathcal{D}(r, r-p)\ N(r-p, t-\Delta t/2) \qquad (3\text{-}17)$$

Thus the amount of species r leached between t and $t + \Delta t$ is approximated as

$$\Delta N(r, t+\Delta t/2) = N(r, t+\Delta t/2)\ \frac{m_o}{\tau}\ \Delta t \qquad (3\text{-}18)$$

Quantity $\Delta N(r, t + \Delta t/2)$ is placed in the undissolved inventory which is given by

$$N_u(r, t+\Delta t/2) = \sum_{p=o}^{N_p(r)} \left\{\mathcal{D}(r, r-p)\ N_u(r-p, t-\Delta t/2)\right\} + \Delta N(r, t+\Delta t/2) \qquad (3\text{-}19)$$

where $N_u(r,t)$ represents the quantity of species r in the undissolved inventory at time t. The quantity of species r which enters solution between t and t + Δt is

$$\Delta N_s(r,\ t+\Delta t/2) = \text{MIN}\ [N_u(r,\ t+\Delta t/2),\ C_s Q \Delta t] \qquad (3\text{-}20)$$

where $\Delta N_s(r,\ t + \Delta t/2)$ is the amount of species r placed in solution between t and t + Δt, C_s is the solubility limit in mass radionuclide per mass fluid, and Q is the fluid flow rate in mass fluid per time.

To model discharge, a 3-dimensional array, F(i, r, r-p), is initially created in a manner similar to the creation of B. Here index i represents a number of grid blocks to the left of the right boundary. Thus, F(i, r, r-p) is the fraction of species r - p in grid block N_x - i + 1 that decays to species r and discharges during Δt. The decay and production factors included in these fractions are altered from those in (3-12) and (3-13) by replacing Δt with the time at which the spatial midpoint of a packet crosses the boundary. Discharge of species r between time t and time t + Δt is then given by

$$\delta(r,\ t+\Delta t) = \sum_{p=o}^{N_p(r)} \sum_{i=1}^{L(r,r-p)} F(i,r,r-p)\ p(N_x - i + 1,\ r-p,\ t) \qquad (3\text{-}21)$$

where $L(r, r-p)$ is the maximum number of grid blocks traversed by any packet that decays from species r - p to species r during Δt. The discharge rate for species r is defined at $t + \Delta t/2$ and is considered constant over Δt. That is,

$$R(r,t+\Delta t/2) = Q\ \delta(r,t+\Delta t) \qquad (3\text{-}22)$$

CHAPTER IV. ERROR ANALYSIS

The Distributed Velocity Method differs from other direct-simulation methods primarily through its grid block mixing feature. Use of this process means that there is no need to track individual particles as is done in the Method of Characteristics and in Monte Carlo techniques. Grid-block mixing thus reduces computer storage requirements and permits tracking chains of radionuclides. Such mixing does, however, introduce some numerical dispersion.

A statistical-numerical method was used to evaluate numerical dispersion introduced by DVM. Thus instead of attempting to evaluate convergence errors theoretically, as was done by Lantz [1971] for the finite-difference method, we exercised DVM on a model problem. Statistical sampling was used to select the various increments and variable values used in such calculations. Comparisons with analytical solutions were then made to determine the numerical dispersion introduced by DVM. Finally, stepwise regression analysis was used to determine a relationship between the numerical dispersion and the input quantities which were varied in the analysis.

The Model Problem. The usual method for making error analyses is to select a simple one-dimensional model problem for analysis. The expectation is, of course, that the numerical errors present in more complex implementations will manifest themselves in a

quantitatively similar manner to to the simplified problem. We also used this strategy. However, in contrast to the theoretical error analysis cited above, ours was a numerical analysis. Thus we had to choose numerical values for our physical problem. We chose a one-dimensional flow system with the length and velocity parameters

$$L = 100{,}000 \text{ ft} \quad \text{and}$$

$$\bar{v} = 1 \text{ ft/yr} \quad . \tag{4-1}$$

These values are not dissimilar from those which might arise in an actual repository evaluation. Within this flow system, we considered transport of a stable, non-retarded contaminant subject to the boundary conditions

$$(x = 0,\ t) = 1 \tag{4-2}$$

$$(x > 0,\ t = 0) = 0 \tag{4-3}$$

Determination of Numerical Dispersion. DVM was used to determine time-dependent discharge from the system described above. The resulting numerical dispersion was then determined analytically as described in this section. Eq. (2-8), when written for the boundary conditions stated above, becomes

$$\frac{\partial \rho}{\partial t} = D \frac{\partial^2 \rho}{\partial x^2} - \bar{v} \frac{\partial \rho}{\partial x} \tag{4-4}$$

where D is related to the velocity $\bar{v}$ by the dispersivity α, i.e.,

$$D = \alpha|\bar{v}| \tag{4-5}$$

For the boundary conditions of Eq. (4-2) and (4-3), the general solution of Eq. (4-4) is

$$\rho(x,t) = \frac{1}{2}\left[\text{erfc}\left(\frac{1}{\sqrt{2}}\,\frac{x-\bar{v}t}{\sqrt{2Dt}}\right) + e^{x\bar{v}/D}\,\text{erfc}\left(\frac{1}{\sqrt{2}}\,\frac{x+\bar{v}t}{\sqrt{2Dt}}\right)\right] \tag{4-6}$$

Our interest in this solution is restricted to one point in the space domain, namely, $x = L$, and a relatively small region of the time domain, namely $t \approx T$ where T is the the mean migration time.

$$T = L/\bar{v} = 100{,}000 \text{ yr.} \tag{4-7}$$

In this case, the second term in Eq. (4-6) is negligible yielding

$$\rho(L,t) \approx \frac{1}{2}\,\text{erfc}\left(\frac{1}{\sqrt{2}}\,\frac{T-t}{(\sqrt{2Dt})/\bar{v}}\right) \tag{4-8}$$

Thus the discharge pulse takes the shape of an error function in which the standard deviation in the time domain of the underlying normal distribution is

$$\sigma_T \approx \frac{\sqrt{2DT}}{\bar{v}} = \frac{\sqrt{2\alpha L}}{\bar{v}} \qquad (4\text{-}9)$$

In order to use Equations (4-8) and (4-9) to interpret results from DVM, the assumption is made that numerical errors inherent in DVM will manifest themselves as numerical dispersion which is indistinguishable from physical dispersion. This means that σ_T must be replaced by an effective standard deviation which includes both numerical and physical dispersion, i.e.,

$$\sigma_T \rightarrow \sigma_{eff} = \frac{\sqrt{2\alpha_{eff} L}}{\bar{v}} \qquad (4\text{-}10)$$

with α_{eff} being the effective dispersivity. Use of the properties of the error function in Eq. (4-8) then yields

$$2\sigma_{eff} = T_{84} - T_{16} \qquad (4\text{-}11)$$

or, from Eq. (4-10)

$$\alpha_{eff} = \left[(T_{84} - T_{16})^2 \bar{v}^2\right] / 8L \qquad (4\text{-}12)$$

Quantities T_{16} and T_{84} are the times at which the discharge rate, as calculated by DVM, reaches 16 and 84 percent of its maximum value. These two times were determined by interpolation of the DVM - generated output and the effective dispersivity was calculated using Eq. (4-12).

Variable Ranges and Distributions. Quantities which were varied in the error analysis of DVM are shown in Table 1. The table displays both the variable ranges and distributions which were chosen. The range of dispersivity values was selected to include values one might find in field measurements. Ranges on the number of intervals in the space and time domain were chosen to span a range of Peclet and Courant numbers which would adequately test DVM. The range of values selected for the number of velocity intervals was also considered adequate to test DVM. Points sampled randomly from a log uniform distribution are distributed uniformly on a logarithmic scale. This means that, in the case of dispersitivity, one would sample as many values on the range (1, 10) as on the range (10, 100). Thus log uniform distributions concentrate point selection toward the low end of the range. The use of log uniform distributions for N_x, N_T and α assured that most calculations were performed with relatively large values of Δx and Δt and small values of α.

Results. Latin Hypercube Sampling [Iman, Helton and Campbell, 1978] was used to select 50 input vectors (N_x, N_T, α, N_v) from the ranges in Table 1. Using the model problem described earlier in this chapter, transport calculations were then performed for each of the 50 input vectors using DVM. Time-dependent discharge rates were interpreted via Eq. (4-12). Effective dispersivity (i.e., the response variable) was fitted using step-wise regression.

Table 1. Variable Ranges of Sensitivity Analysis of DVM Numerical Dispersion

Variable	(Range)	Assumed Distribution
N_X*	(25, 1000)	Log Uniform
N_T*	(25, 1000)	Log Uniform
N_V	(3, 10)	Uniform
α	(1, 500)	Log Uniform

N_X = number of spatial intervals

N_T = number of time intervals per migration time

N_V = number of velocity intervals

α = dispersivity (ft)

*The equivalent range for Δx is (100, 4000) ft.

*The equivalent range for Δt is (100, 4000) yrs.

Results are presented in Table 2. The regression sum of squares (R^2) value of 0.91 indicates a good fit was achieved. The R^2 value, if multiplied by 100, can be interpreted as the percentage of variation in the response variable (i.e., effective dispersivity) which is explained by the fitted expression. The standardized regression coefficient provides an indication of the relative importance of selected input variables in explaining output variation. Thus the ratio N_T/N_x was responsible for most of the variation in effective dispersivity. Note that the number of velocity intervals (N_v) was not selected as a significant variable. The fitted expression for α_{eff} which is indicated in Table 2 is the following:

$$\alpha_{eff} = 61.2 \frac{N_T}{N_x} + \frac{4.95 \times 10^5}{N_x^2} + 0.859\ \alpha - 26.32 \qquad (4\text{-}13)$$

For comparison with other numerical schemes, it is desirable to recast this equation in several different forms. For example, the grid-block or element Peclet number is important for finite-difference or finite-element calculations. In the latter, and in centered-in-space implementations of the former, the relation

$$p = \frac{\Delta x}{\alpha} \leq 2 \qquad (4\text{-}14)$$

Table 2. Stepwise Regression Analysis Results

Variable Selected	Regression Coefficient	Standardized Regression Coefficient
N_T/N_X	61.2	0.617
$1/N_X^2$	4.95×10^5	0.441
α	0.859	0.258

Intercept = -26.3

$R^2 = 0.91$

must be maintained to prevent spatial oscillations. It is useful, then to restate Eq. (4-13) in terms of the Peclet number

$$\frac{\alpha_{eff}}{\alpha} = 6.12 \times 10^{-4} \left(\frac{L}{v\Delta t}\right) p + 4.95 \left(\frac{\Delta x}{L}\right) p - 2.63 \times 10^{-4} \left(\frac{L}{\alpha}\right) + 0.859 \qquad (4\text{-}15)$$

The results shown in Figures 4(a) - 4(d), obtained from Eq. (4-15), more clearly illustrate the effects of Peclet number on the numerical dispersion introduced by DVM. In generating these results, the fitted response surface was not used outside the variable ranges shown in Table 1. This explains, for example, why the maximum value of Δx is 500 for $p = 1$. Similar restrictions will be apparent in other results produced from the fitted response surface.

The results shown in Figure 4(a) to 4(d) indicate that as the Peclet number increases, the space step may be decreased or the time step increased to reduce numerical dispersion. The limiting value of Δt may be determined by the resolution desired for the discharge curve. For instance, one might require

$$\Delta t \leq \sigma_t = \sqrt{2\alpha L} \,/\bar{v} \qquad (4\text{-}16)$$

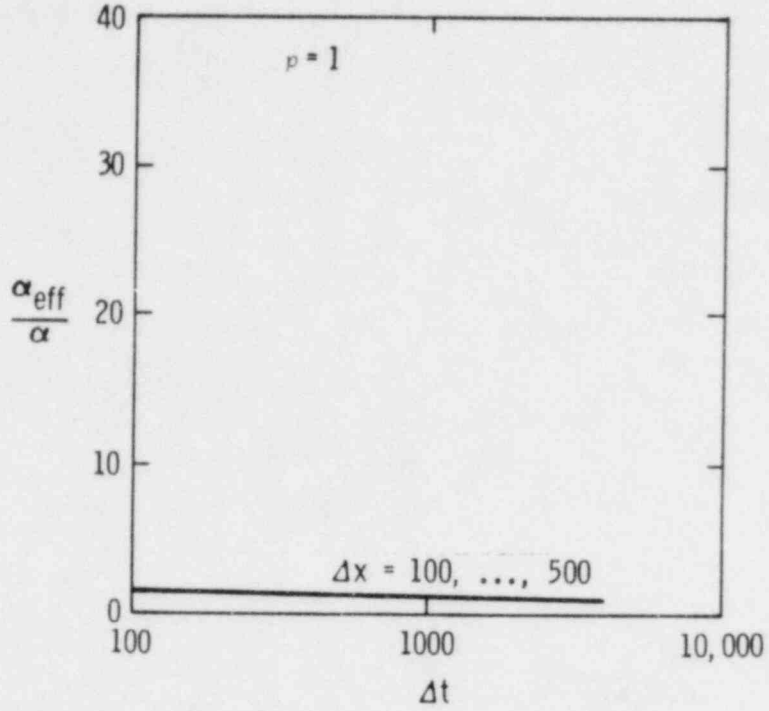

Figure 4a. Effective Dispersivity for Several Values of Peclet Number

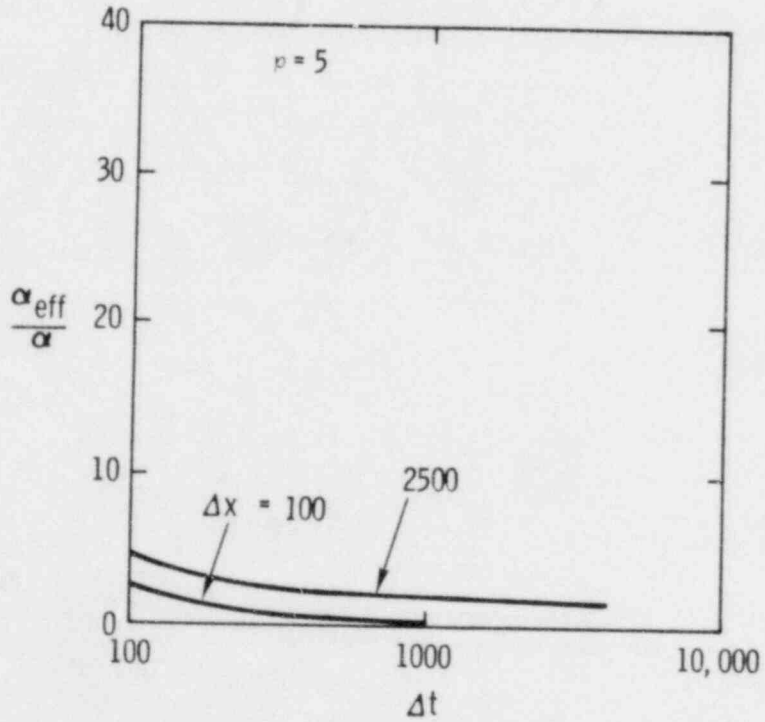

Figure 4b. Effective Dispersivity for Several Values of Peclet Number

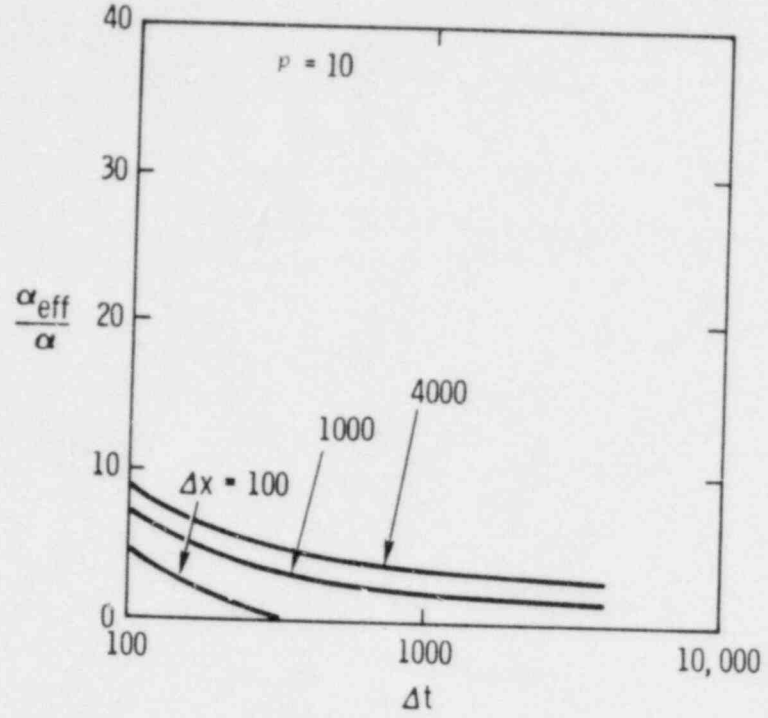

Figure 4c. Effective Dispersivity for Several Values of Peclet Number

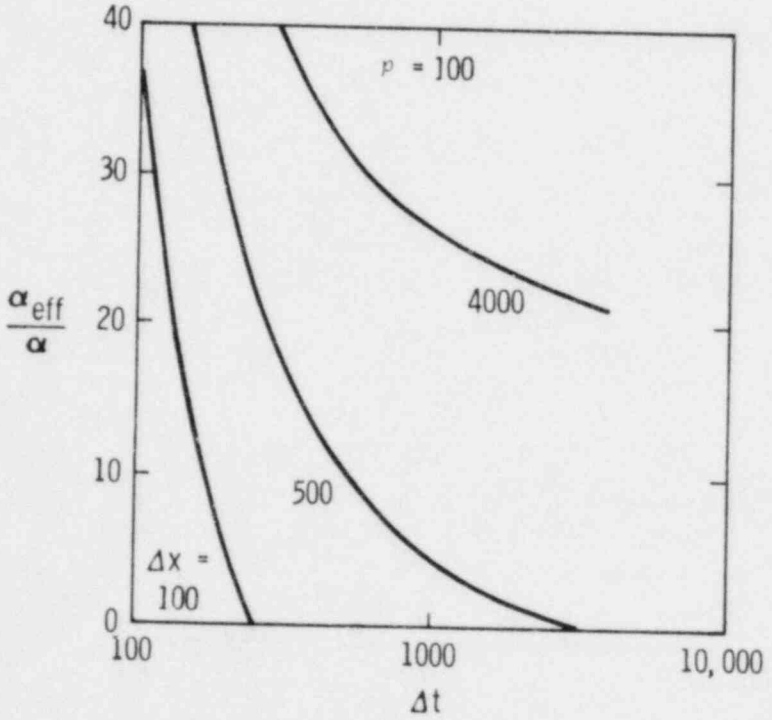

Figure 4d. Effective Dispersivity for Several Values of Peclet Number

For the model problem and range of dispersivity considered in this error analysis, the range of values for σ_t is

$$450 \leq \sigma_t \leq 10{,}000 \text{ yr} \tag{4-17}$$

For calculations involving radioactive decay, one may require

$$t \leq T_{1/2} \tag{4-18}$$

where $T_{1/2}$ is the half life of the shortest-lived isotope.

It should be noted that for large values of P and small values of Δx, the fitted response surface may predict values for α_{eff}/α less than 1. This does not indicate problems with DVM but rather that the response surface fit may not be adequate over the full range of all variables. However, in the 50 transport calculations, which form the basis of this error analysis, the smallest observed value of α_{eff}/α was 0.7.

Effective dispersivity, as given by Eq. (4-13) may also be expressed in terms of Courant numbers as follows:

$$\frac{\alpha_{eff}}{\alpha} = 6.12 \times 10^{-4} \left(\frac{L}{\alpha}\right) \left(\frac{1}{C}\right) + 4.95 \frac{\Delta x}{L} \frac{\Delta x}{\alpha} - 2.63 \times 10^{-4} \left(\frac{L}{\alpha}\right) + 0.859 \tag{4-19}$$

The Courant number, like the Peclet number, is significant for finite difference and finite element formulations. For centered-in-time finite difference implementations, it is limited (to first order) as follows:

$$c = \frac{v\Delta t}{\Delta x} \leq 2 \qquad (4\text{-}20)$$

Eq. (4-19) shows an inverse dependence of effective dispersivity on Courant number which is at variance with finite-difference and finite-element formulations. Thus rather than bounding the Courant number from above, as in Eq. (4-20), it apparently must be bounded from below in DVM.

Figures 5(a) - 5(d) show the relationships between the variables c, Δx and α which control numerical dispersion for a given value of α. To lower numerical dispersion either Δx must be decreased or c must be increased. Considering the direct dependence of Courant number on Δt, however, this prescription is identical to the one observed previously for the Peclet-number representation. The direct dependence of numerical dispersion on Peclet number and thus on grid-block size is a rather conventional relation, compared to other methods. However, the inverse dependence of numerical dispersion on Courant number and thus on time increment is quite irregular. The implication is that, consistent with the desired resolution [Eq. (4-16)] and the shortest half-life [Eq. (4-18)], the time increment should be made as large as possible. This has the

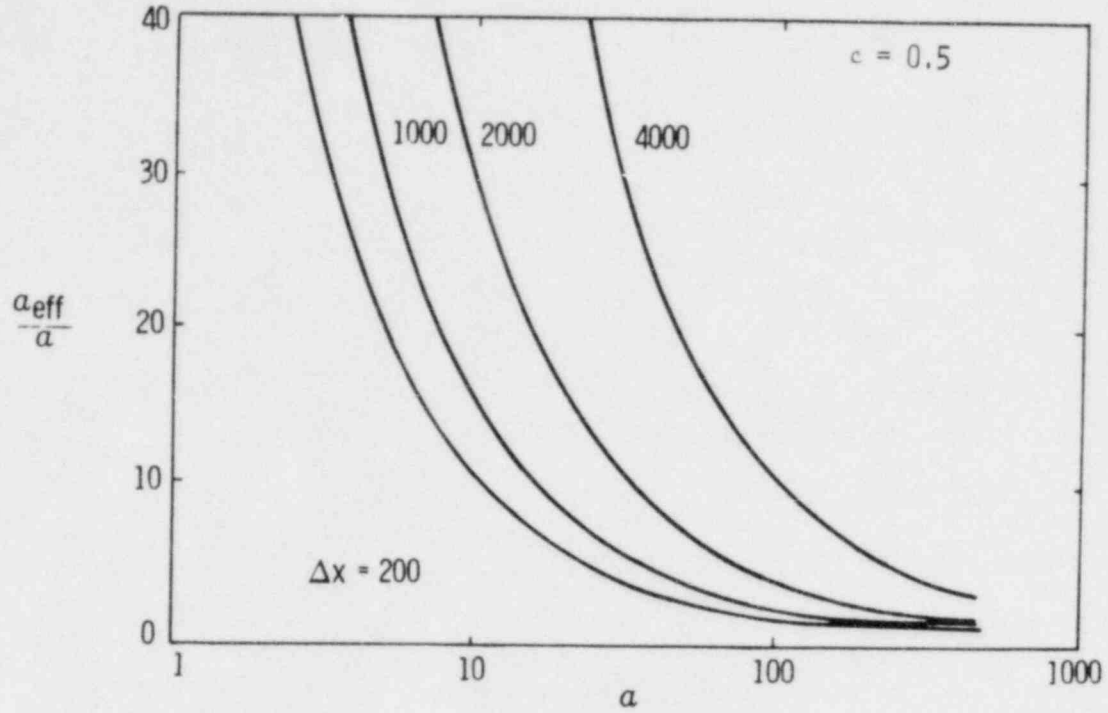

Figure 5a. Effective Dispersivity for Several Values of Courant Number

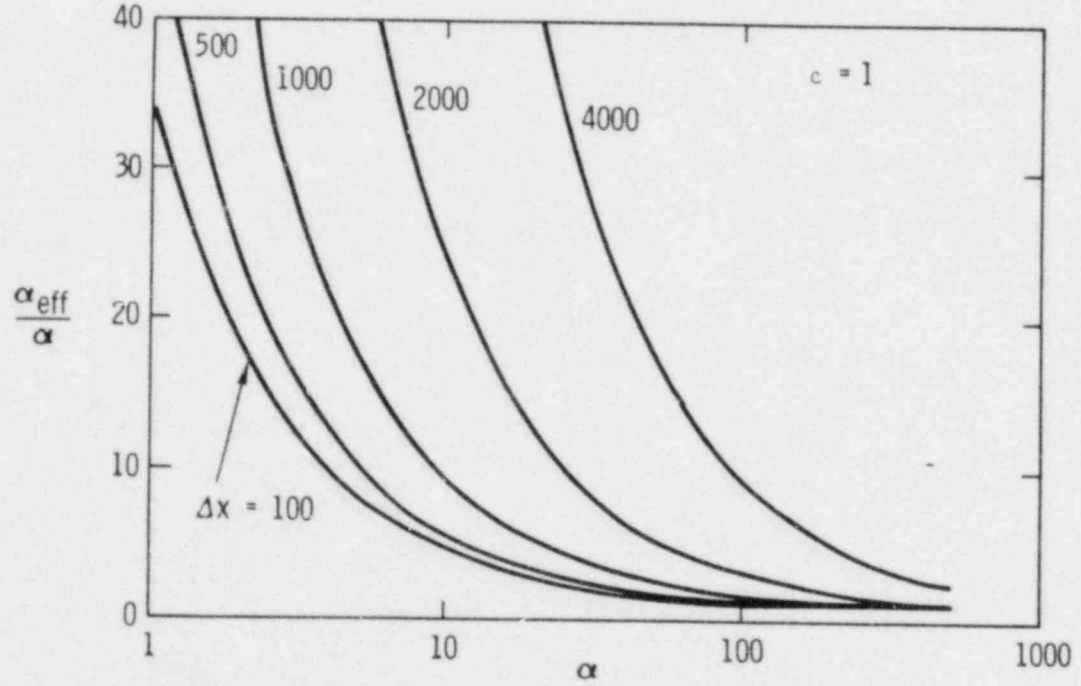

Figure 5b. Effective Dispersivity for Several Values of Courant Number

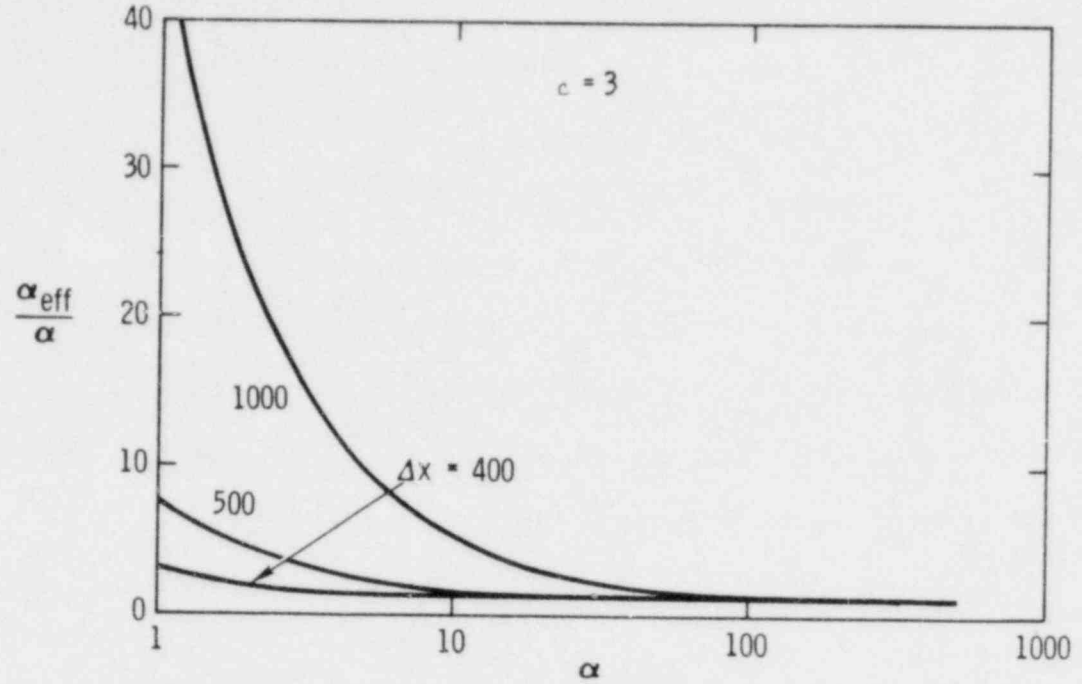

Figure 5c. Effective Dispersivity for Several Values of Courant Number

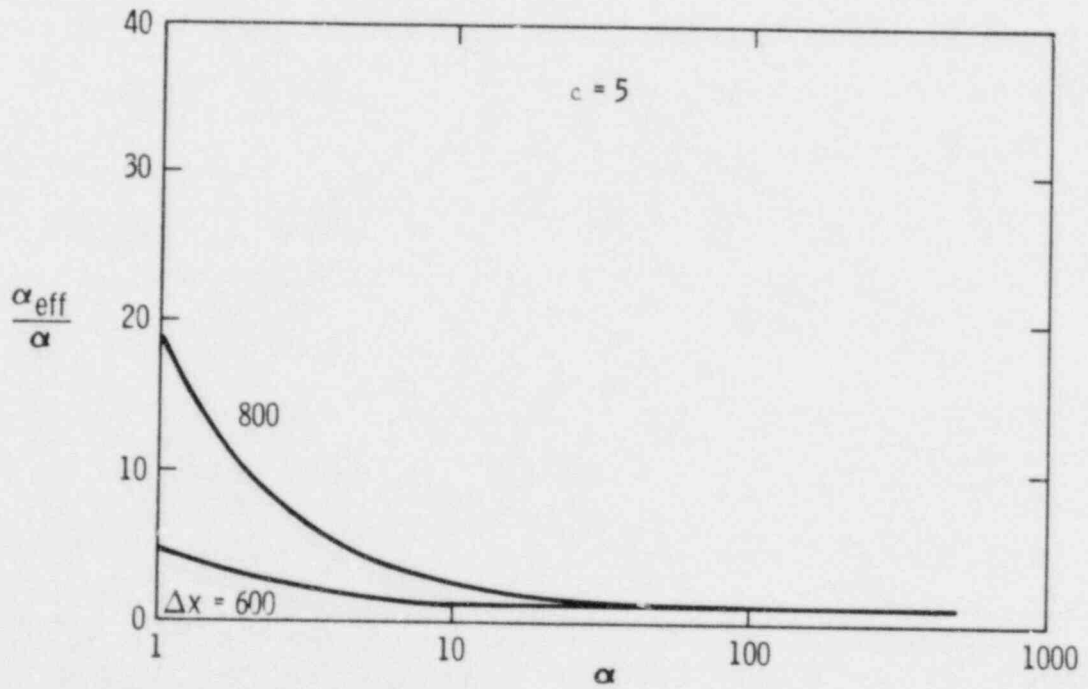

Figure 5d. Effective Dispersivity for Several Values of Courant Number

dual benefit of decreasing numerical dispersion and decreasing computer running time.

The importance of small grid blocks and large time steps can be understood by considering the numerical implementation of DVM. Contaminant transport is advanced through each time step by application of the Green's function matrix. At the end of each time step, contaminant concentrations are repartitioned among grid blocks. Clearly this repartitioning process would introduce less numerical dispersion in a fine grid-block structure than in a coarse one. Furthermore, large time steps imply that this repartitioning takes place fewer times, thus reducing numerical dispersion.

Before concluding this chapter, it is of interest to examine some of the breakthrough curves generated in the error analysis. We select a series having high Peclet numbers and examine the effect of Courant number on effective dispersivity. As stated earlier, for a given Peclet number, the effective dispersivity can be reduced by increasing the Courant number. Figures 6, 7 and 8 illustrate this property of DVM. In Figure 6, despite the small dispersivity (α = 1.5 ft) and large Peclet number (p = 89), the comparison between DVM and the analytic solution is excellent. The reason for this good comparison is the relatively large Courant number ($c \approx 7$). In Figure 7, the Courant number is smaller ($c \approx 1$) than in Figure 6 and, as expected, the numerical dispersion has increased. Nevertheless,

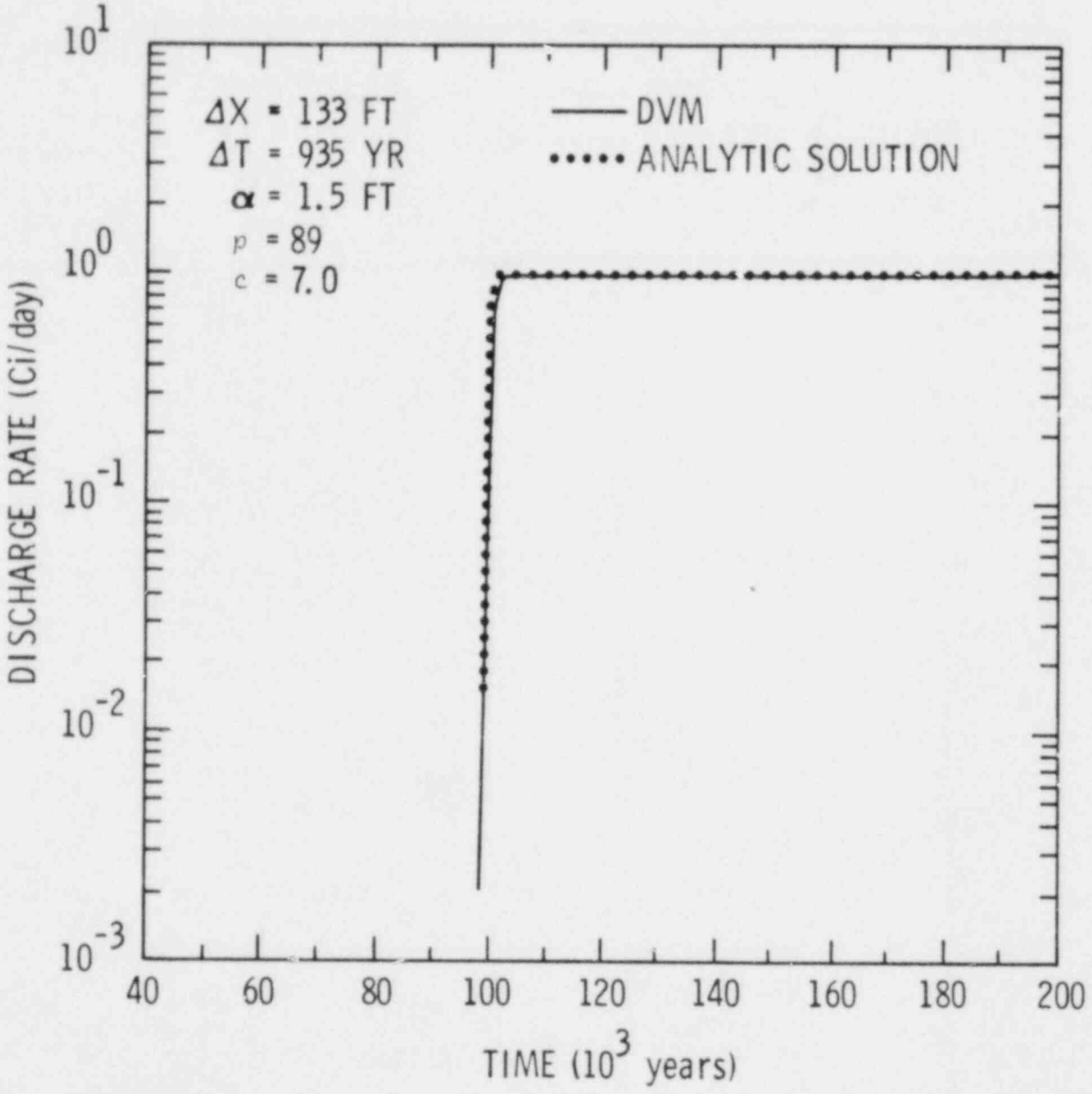

Figure 6. Comparisen Between DVM and Analytic Solution

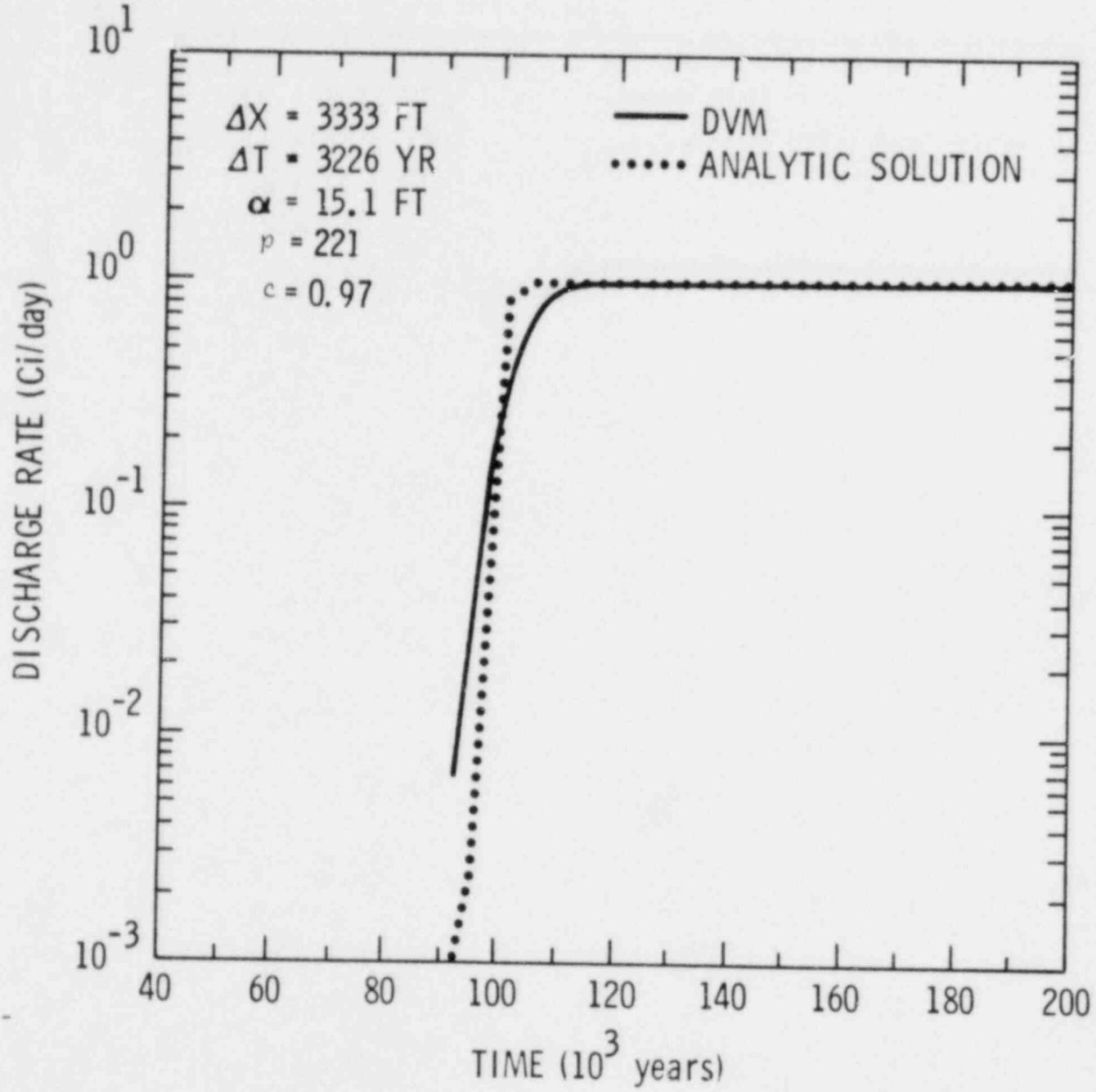

Figure 7. Comparison Between DVM and Analytic Solution

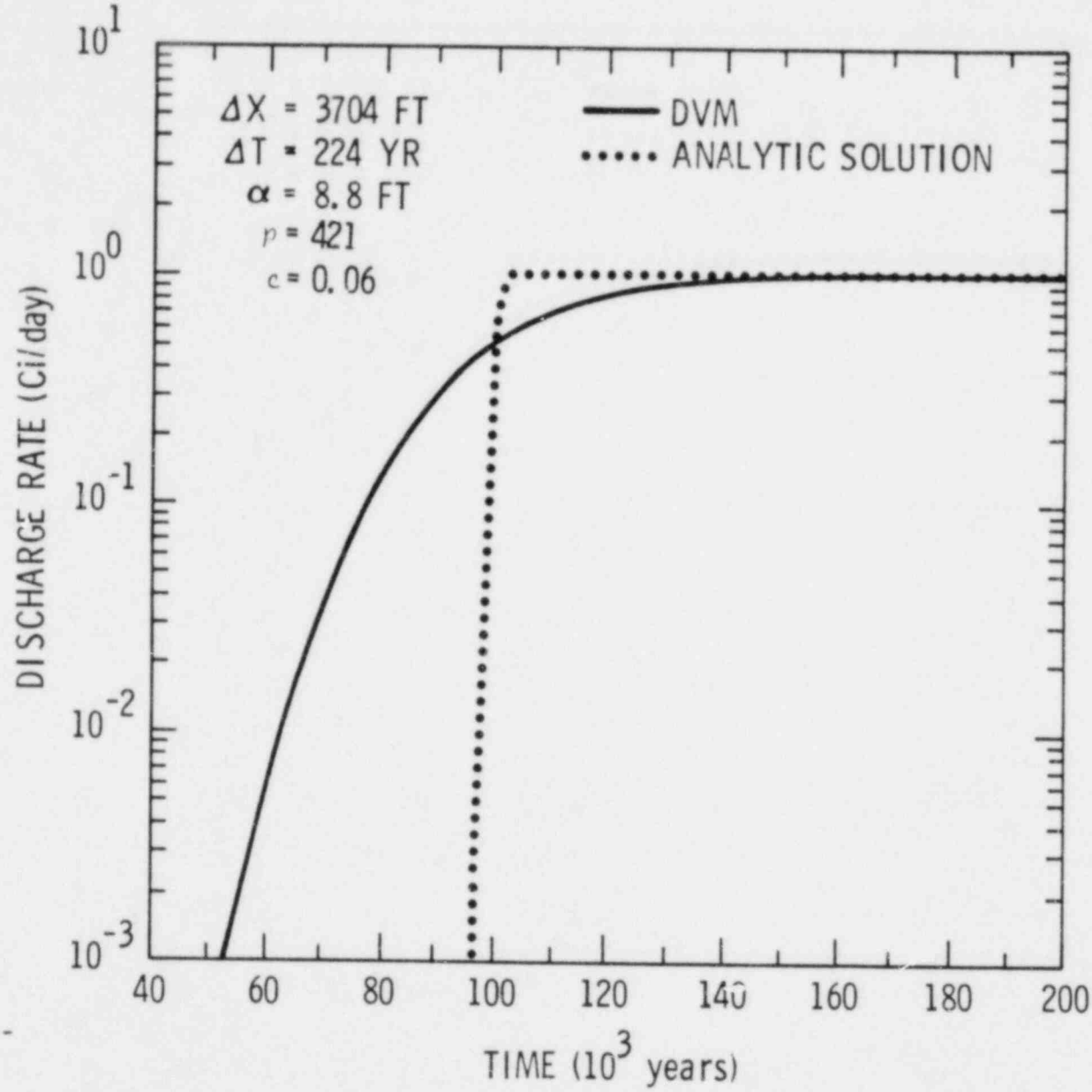

Figure 8. Comparison Between DVM and Analytic Solution

the numerical errors apparent in Figure 7 would be tolerable in most practical applications.

The results shown in Figure 8 are particularly significant in that, among all the 50 calculations whose parameters span the ranges exhibited in Table 1, this particular one displayed the largest effective dispersivity. This result is not surprising considering the small dispersivity (α = 8.8), the large Peclet number (p = 421) and the small Courant number (c = 0.06).

CHAPTER V. COMPARISON OF DVM WITH OTHER METHODS

In the last chapter on error analysis, several comparisons were made between DVM and an analytic solution. The objective there was to answer the question: "How does one use the DVM technique?" In other words, what space and time steps should be used to control numerical dispersion? This chapter addresses the question: "Why should one use DVM?" There are various other available methods. We have chosen three of them for comparison, specifically an analytic implementation (computer code GETOUT [DeMier, et al., 1979]), a Method of Characteristics (MOC) code [INTERA, 1979], and the finite difference (FD) computer code SWIFT [Dillon, Lantz and Pahwa, 1978]. It should be pointed out that both of the numerical methods just mentioned are extendable to higher dimensions, although three dimensions do present a storage problem for MOC. The DVM, the authors feel, may be extended to higher dimensions, but, as yet, this is unproven. Our objective here is to show that, even in one dimension, an important role exists for DVM in risk calculations because of its broad range of applicability in terms of Peclet numbers, radioactive chains, leach- or solubility-limited sources, and computer efficiency.

DVM is first compared with the Method of Characteristics [INTERA, 1979] for a decaying isotope. Parameters of the comparison calculations are shown in Table 3. Results of the comparisons are shown in Figure 9 where an analytical solution

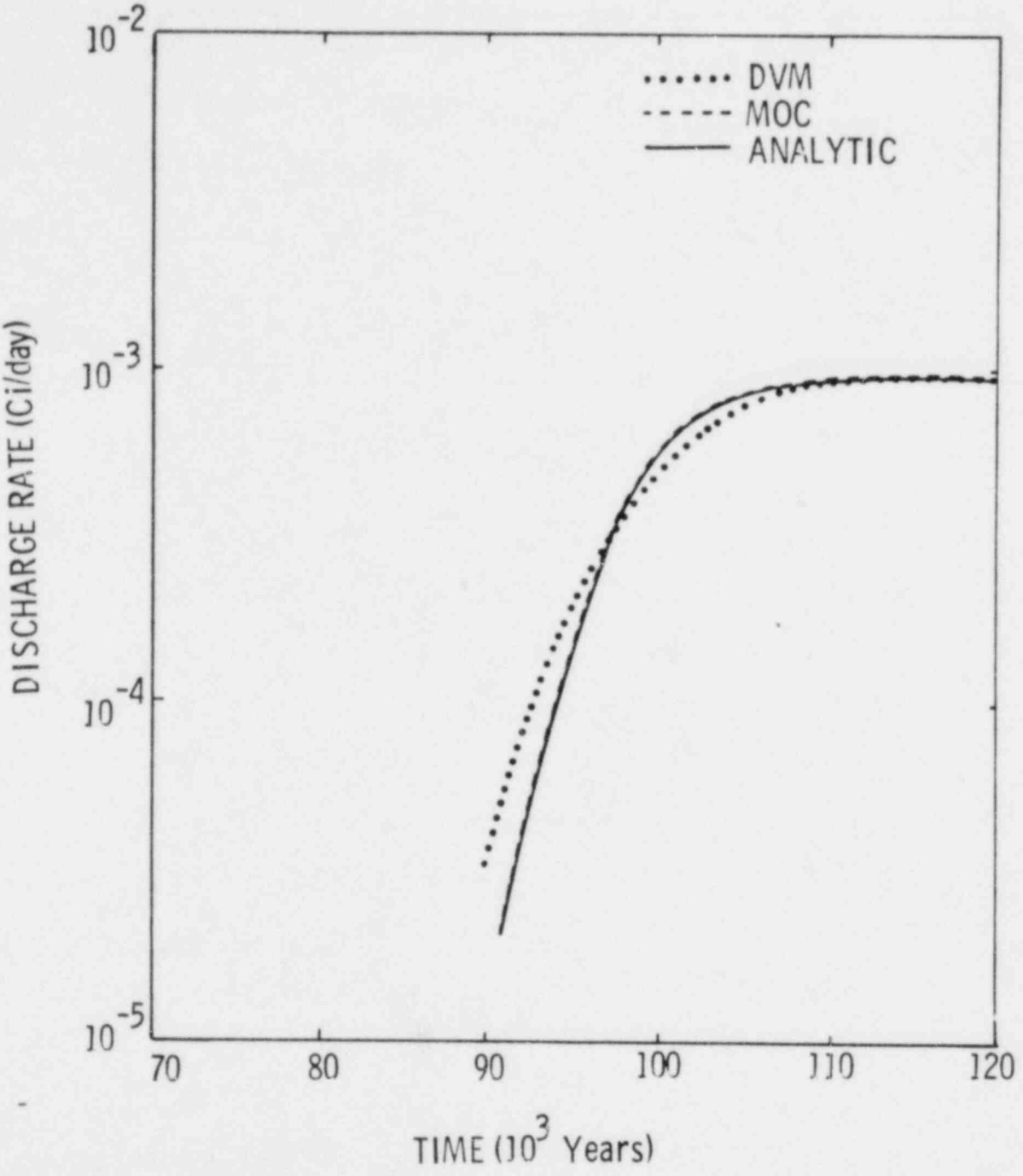

Figure 9. Comparison Between DVM and MOC

is included for reference purposes. No results from finite difference are shown because of the relatively large Peclet number. The results indicate that DVM has introduced some numerical dispersion ($\alpha_{eff}/\alpha \approx 1.5$). Any numerical dispersion introduced by MOC appears negligible. The fact that DVM introduced some numerical dispersion is not surprising in light of the small Courant number (c = 1). In fact, such results could have been anticipated by referring to Figure 5.B. Furthermore, it is clear from Figure 5.B and Eq. (4-19) that the numerical dispersion could be further reduced by increasing the time step.

Problem parameters for the second comparison calculation are presented in Table 4. In this case a radioactive decay chain consisting of three species is considered. A source inventory of 1000 curies was used for each species. The rather large contrasts in half lives and retardation factors were taken to assure a strenuous test of DVM.

As indicated in Table 4, a time step of 4000 years was used throughout the DVM calculation. In the finite difference calculation, however, a time step of 400 years was used for 250,000 years to control the Courant number for isotope C. Once discharge of isotope C was effectively completed, the time step was increased to 4000 years to avoid excessive computer costs. The 4000 year time step adequately controlled the Courant number for isotope A. As isotope B is in equilibrium with A, the fact that the time step criterion is violated for

Table 3. Problem Parameters for Comparison of DVM and MOC

$L = 100{,}000$ ft	$x = 1{,}000$ ft
$\alpha = 100$ ft	$t = 1{,}000$ yr
$\bar{v} = 1.0$ ft/yr	$p = 10$
$T_{1/2} = 10^4$ yr	$c = 1$

Table 4. Problem Parameters for Comparison of DVM and Finite Difference (FD)*

Isotope	Half Life (years)	Retardation Factor	Courant Number DVM	Courant Number FD
A	10^6	100	2.0	0.2 (2.0)#
B	10^3	1	200	20 (200)#
C	10^7	10	20	2.0 (20)#

	DVM	FD
L = 100,000 ft		
α = 100 ft	Δx = 200 ft	200 ft
$\bar{v}$ = 10 ft/yr	Δt = 4000 yr	400 (4000)# yr
$\tau = 10^5$ yr		

*A centered-in-space, centered-in-time implementation was used with Δx = 200 ft and Δt varied as described below.

#The time step in the Finite Difference calculation was set at 400 years until isotope C discharged (about 250,000 years) then was changed to 4000 years.

isotope B does not introduce excessive numerical error. Results of the comparison calculations are shown in Figure 10. An analytical solution obtained from the GETOUT model [DeMier, et al., 1979] is also shown in Figure 10.

The message of Figure 10 is twofold. First, results from MOC are not presented since no implementation of that technique (or of any other particle-tracking technique) was available which was capable of treating radionuclide chains. Secondly, there is the matter of computer efficiency. The FD code, even with controlled violation of the centered-in-time criteria [c.f., Eq. (1-2b)], took 125 seconds of CDC 7600 time as compared to 20 seconds of CDC 7600 time for the DVM results.

In the final comparison calculation, the problem parameters listed in Table 4 were used with the exception that the retardation factor for isotope A was increased to 1000 and the leach time (τ) was increased to 10^6 years. In this case DVM was only compared to an analytic solution, as the computer cost for a finite difference calculation would have been prohibitive. Results are shown in Figure 11. The comparison between DVM and the analytic solution is excellent.

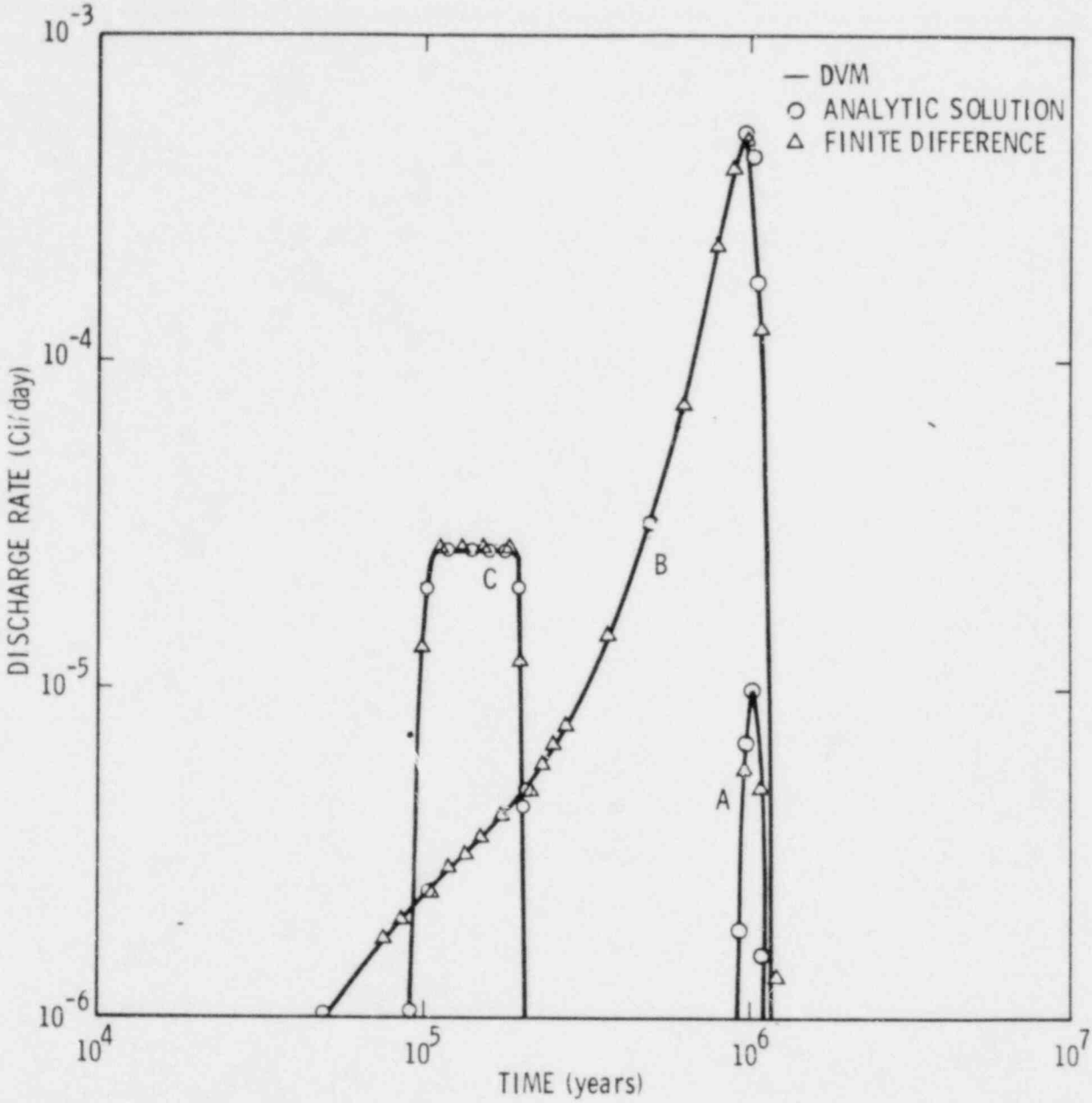

Figure 10. Comparison Between DVM and Finite Difference Model

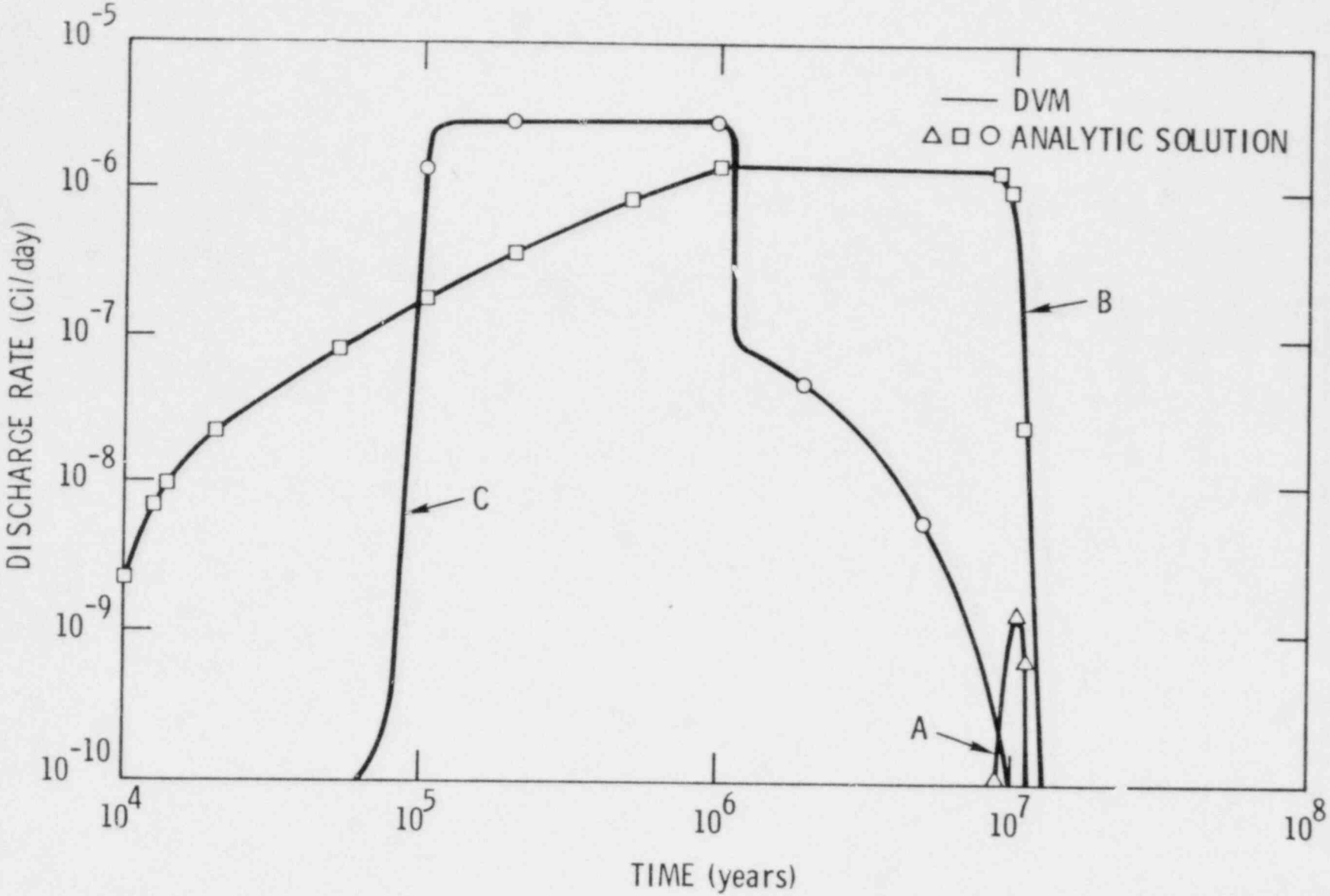

Figure 11. Comparison Between DVM and Analytic Solution

CHAPTER VI. SUMMARY AND CONCLUSIONS

A new method has been proposed for treating convective-dispersive transport. The motivation for developing this technique arises from the demands of performing a risk assessment for a nuclear waste repository. These demands include computational efficiency, the ability to handle chains of decaying radionuclides with rather extreme contrasts in solution velocities and half lives, and an ability to treat both leach-and solubility-limited sources. To the extent it has been tested to date, the Distributed Velocity Method (DVM) appears to meet these demands.

DVM directly simulates contaminant migration in groundwater by simulating the movement of ensembles of representative particles. The spatial extent of an ensemble is taken to be one grid block. Dispersion is treated by assigning a velocity distribution to these particle ensembles. Both the basic theory and the numerical implementation are presented in this document.

Because DVM treats ensembles of particles rather than individual particles, as is done by other direct simulation methods, radioactive decay chains can be transported without requiring excessive computer storage. However, the grid-block averaging feature in DVM does introduce some numerical dispersion. Such dispersion is analyzed in this report using statistical techniques. Statistical sampling and step-wise regression analysis are used to determine an analytical formula for the effective

dispersions in terms of the most important parameters controlling this dispersion. This formula is plotted graphically to demonstrate its meaning and should be quite straightforward to apply in practice. The conclusions of the error analysis are twofold. First the dependence of numerical dispersion upon Peclet number is regular in that such dispersion increases as Peclet number increases. Secondly, the dependence upon Courant numbers is irregular in that the numerical dispersion decreases as the Courant number increases. The implication of the latter point is that numerical error may be decreased and, at the same time, the technique may be made more efficient by simply increasing the time step. The desired resolution of the discharge pulse and the half lives of the radioactive species being transported impose maximum conditions in the time step.

Finally calculations from DVM were compared with several other techniques to exhibit the areas in which it complements those methods. Comparisons were made with state-of-the-art implementations of analytic, Method-of-Characteristics (MOC) and finite-differences (FD) computer models. Only one dimension was considered since DVM has not yet been extended to more than one dimension and since the analytic code also treats only one dimension. Even so, applications involving decay chains, solubility limitation, Peclet numbers $p > 2$, and applications requiring high efficiency were either not covered or poorly covered by analytic, MOC, and FD techniques. Such applications will occur frequently in risk analyses of depository sites.

We therefore feel that DVM is an important complement to existing transport models.

NOMENCLATURE

B	Coefficient matrix for advancing transport solution by Δt (dimensionless)
c	Courant number (dimensionless)
C_s	Solubility limit (M/M)
D	Dispersion coefficient (L^2/T)
$\mathcal{D}$	Radioactive decay/production fraction (dimensionless)
F	Fractional discharge matrix (dimensionless)
G	Green's function in coordinate space (L^{-1})
$\mathcal{G}$	Green's function in velocity space ($(L/T)^{-1}$)
K_r	Retardation factor for isotope r (dimensionless)
L	Transport path length (L)
$\mathcal{M}$	Geometrical mixing fraction (dimensionless)
m	Mass of waste matrix (M)
m_o	Initial mass of waste matrix (M)
N	Mass fraction of a radioactive species in the waste matrix (M/M)
N_u	Mass of radioactive species in the undissolved inventory (M)
P	General velocity distribution ($(L/T)^{-1}$)
p	Peclet number (dimensionless)
Q	Fluid flow rate (M/T)
R	Radionuclide discharge rate (M/T)
S	Source rate (M/T)
T	Travel time (T)
T_{16}	Time for discharge rate to reach 16 percent of peak (T)
T_{84}	Time for discharge rate to reach 84 percent of peak (T)

t	Time (T)
v	Velocity (L/T)
$\bar{v}$	Average velocity (L/T)
W	Velocity subgroup weight from velocity distribution (dimensionless)
x	Distance (L)

Greek Variables

α	Dispersivity (L)
α_{eff}	Effective dispersivity (L)
ΔN	Amount of radioactive species leached in time step Δt (M)
ΔN_s	Amount of radioactive species entering solution in time Δt (M)
δ	Discharge of radioactive species in time step Δt (M/M)
λ	Decay constant (T^{-1})
ρ	Radionuclide concentration
ρ_o	Radionuclide concentration arising from propagation of initial conditions
σ_{eff}	Standard deviation obtained from calculated breakthrough curve (T)
σ_t	Standard deviation in analytic breakthrough curve (T)
σ_x	Standard deviation in spatial Green's function (L)
σ_v	Standard deviation in velocity Green's function (L/T)
τ	Leach time (T)

Subscript Variables

l	Maximum number of grid blocks traversed by a packet which decays from species r-p to species r in Δt
N_B	Number of donor grid blocks which contributed to a receiver grid block

N_p Number of radioactive parents

N_T Number of time increments

N_v Number of velocity intervals

N_x Number of grid blocks

References

Ahlstrom, S. W., Foote, H. P., Arnett, R. C., Cole, C. R., and Serne, R. J., Multicomponent Mass Transport Model: Theory and Numerical Implementation (Discrete-Parcel-Random-Walk Version), Battelle Pacific Northwest Laboratories, BNWL-2127.

Ames, W. F., Numerical Methods for Partial Differential Equations, Academic Press, 1977.

Campbell, J. E., Dillon, R. T., Tierney, M. S., Davis, H. T., McGrath, P. E., Pearson, F. J., Shaw, H. R., Helton, J. C., and Donath, F. A., Risk Methodology for Geologic Disposal of Radioactive Waste: Interim Report, NUREG/CR-0458 and SAND78-0029, Sandia Laboratories, Albuquerque, NM, 1978.

DeMier, W. V., Cloninger, M. O., Burkholder, H. C., and Liddell, P. J., GETOUT - A Computer Program for Predicting Radionuclide Decay Chain Transport Through Geologic Media, Pacific Northwest Laboratory Report PNL-2970, 1979.

Dillon, R. T., Lantz, R. B. and Pahwa, S. B., Risk Methodology for Geologic Disposal of Radioactive Waste: The Sandia Waste Isolation Flow and Transport (SWIFT) Model, Sandia Report SAND78-1267 and NRC Report NUREG/CR-0424, 1978.

Gardner, A. O., Jr., Peaceman, D. W., and Pozzi, A. L., Jr., Numerical Calculation of Multidimensional Miscible Displacement by the Method of Characteristics, Soc. Pet. Eng. Jour. (March, 1964) 26.

Iman, R. L., Helton, J. C., and Campbell, J. E., Risk Methodology for Geologic Disposal of Radioactive Waste: Sensitivity Analysis Techniques, SAND78-0912, Sandia Laboratories, Albuquerque, NM (1978).

INTERA, 1979, private communication of results from INTERA's Method-of-Characteristics code.

Jones, R. B., and Campbell, J. E., The Mathematical Relationship between the Phase-Space-Time-Evolution Method and the Neutron Transport Equation, Transport Theory and Statistical Physics, 7 (1 & 2), 33-50, (1978).

Lantz, R. B., Quantitative Evaluation of Numerical Diffusion (Trancation Error), Soc. Pet. Eng. Journ, September 1971).

Lester, D. H., Jansen, G., and Berkholder, H. C., Migration of Radioactive Chains Through an Adsorbing Medium, AICKE Symposium Series 152, Adsorption and Ion Exchange, 71: 202.

Noble, B., Applied Linear Algebra, Prentice-Hall, 1969.

Pinder, G. F., and Gray, W. G., Finite Element Simulation in Surface and Subsurface Hydrology, Academic Press, 1977.

Price, H. S., Varga, R. S., and Warren J. E., Application of Oscillation Matrices to Diffusion-Convection Equations, J. of Math. and Phys., V. 45, 1966, pp. 301-311.

Schwartz, F. W., Macroscopic Dispersion in Porous Media: The Controlling Factors, Water Resources Research, Vol. 13, No. 4, 1977, pp. 743-752.

Tang, D. H. E., 1980a, private communication.

Tang, D. H. E., 1980b, to be published.

DISTRIBUTION:

U.S. Nuclear Regulatory Commission
NRC Standard Distribution GF (375 cys)
Division of Document Control
Distribution Services Branch
7920 Norfolk Avenue
Bethesda, MD 20014

ACRS Subcommittee on Waste Management (25)
U.S. Nuclear Regulatory Commission
Washington, DC 20555
Attn: R. E. McKinley, H-1016

U.S. Nuclear Regulatory Commission (10)
Office of Nuclear Materials Safety
and Safeguards
Washington, DC 20555
Attn: W. J. Dircks, Director, 958-SS
For: J. Martin, Director
M. Bell, 958-SS
J. Bunting, 958-SS
H. Lowenberg, 958-SS
D. Nussbaumer, 958-SS
R. Boyle, 958-SS
J. Malaro, 958-SS
L. Rossbach, 958-SS
M. Knapp, 958-SS

U.S. Nuclear Regulatory Commission (25)
Probabilistic Analysis Staff
Office of Nuclear Regulatory Research
3106 MNBB
Washington, DC 20555
Attn: R. Bernero, Director
F. Rowsome, Deputy Director
M. Cullingford (22)
W. Vesely

Division of Safeguards, Fuel Cycle and
Environmental Research (2)
Office of Nuclear Regulatory Research
U.S. Nuclear Regulatory Commission
Mail Stop 1130SS
Washington, DC 20555
Attn: F. Arsenault
C. Jupiter

U.S. Nuclear Regulatory Commission (4)
Office of Standards Development
NL 5650
Washington, DC 20555
Attn: N. Costanzi
E. Conti
C. Roberts
P. Conella

DISTRIBUTION (cont'd):

U.S. Congress
Office of Technical Assessment
Washington, DC 20510
Attn: T. Cotton

U.S. Department of Energy (2)
B-107
Washington, DC 20545
Attn: C. Heath, Actg Director,
Div. of Waste Isolation
S. Meyers, Director, Office
of Nuclear Waste Management

U.S. Department of Interior (2)
U.S. Geologic Survey
345 Middlefield Road
Menlo Park, CA 94025
Attn: H. R. Shaw

Los Alamos Scientific Laboratory (2)
Division S1
Los Alamos, NM 87545
Attn: M. Johnson, MS 606
R. Beckman, MS 606

Science Applications, Inc. (2)
Five Palo Alto Square
Palo Alto, CA 94304
Attn: R. Erdman
R. Fullwood

Lawrence Livermore Laboratory (2)
P. O. Box 808
Livermore, CA 94550
Attn: A. Kaufman, L-156
D. Isherwood, L-224

U.S. Department of Interior (5)
U.S. Geologic Survey
P. O. Box 25046
Denver Federal Center
Denver, CO 80225
Attn: D. Leap, Nuclear Hydrology Project, WRD, MS 416
W. S. Twenhofel, Chief, Special Projects Branch
R. Waddell, Nuclear Hydrology Project, WRD, MS 416
D. B. Grove
L. F. Konikow

U.S. Department of Interior (4)
U.S. Geologic Survey
National Center
Reston, VA 22092
Attn: N. Trusk

DISTRIBUTION (cont'd):

U.S. Environmental Protection Agency
Office of Radiation Programs
AW-459
Washington, DC 20464
Attn: D. Egan

Allied General Nuclear Services
P. O. Box 847
Barnwell, SC 29812
Attn: A. L. Ayers
Assistant to the President

American Nuclear Energy Council
1750 K Street, NW, Suite 300
Washington, DC 20006

Texas Tech University
College of Business Administration
P. O. Box 4320
Lubbock, TX 79409
Attn: W. J. Conover

Texas Tech University
Department of Mathematics
P. O. Box 4319
Lubbock, TX 79409
Attn: J. M. Davenport

General Electric Company
175 Curtner Avenue, MC 851
San Jose, CA 95125

Harvard University
Pierce Hall, Room 115
Cambridge, MA 02134
Attn: M. Stack

The Analytical Sciences Corporation
6 Jacob Way
Reading, MA 01867
Attn: J. W. Bartlett
C. Koplik

Harvard University
Physics Department
Cambridge, MA 02138
Attn: R. Wilson

Intera Environmental Consultants (12)
11999 Katy Freeway
Houston, TX 77079
Attn: R. Lantz
J. Pearson
J. Campbell (5)
M. Reeves (5)

DISTRIBUTION (cont'd):

Los Alamos Technical Associates
PO Box 410
1553 Myrtle Street
Los Alamos, NM 87544
Attn: S. E. Logan

Natural Resources Defense Council, Inc.
2345 Yale Street
Palo Alto, CA 94306
Attn: T. Lash

Nuclear Fuel Services
6000 Executive Blvd., Suite 600
Rockville, MD 20852
Attn: W. J. Lewis

Radiation Research Association
3550 Hulen Street
Fort Worth, TX 76107
Attn: R. M. Rubin

Science Applications, Inc. (2)
1200 Prospect Street
PO Box 2351
La Jolla, CA 92037
Attn: L. Simmons
E. Straker

Science Applications, Inc.
1385 George Washington Way
PO Box 857
Richland, WA 99352
Attn: M. J. Szulinski

Swedish Embassy (2)
600 New Hampshire Avenue, NW
Washington, DC 20037
Attn: Lars G. Larson

Office of Nuclear Waste Isolation
Battelle Memorial Institute
505 King Avenue
Columbus, OH 43201
Attn: H. C. Burkholder

The University of Arizona
Department of Hydrology and Water Resources
Tucson, AZ 85721
Attn: D. R. Davis

DISTRIBUTION (cont'd):

University of California
Chemical, Nuclear, and Thermal Engineering Dept.
5532 Boelter Hall
Los Angeles, CA 90024
Attn: G. Apostolakis

University of Pittsburgh
Physics Department
Pittsburgh, PA 15260
Attn: B. Cohen

University of Rhode Island
Graduate School of Oceanography
Kingston, RI 02881
Attn: G. R. Heath

University of Tennessee
Department of Nuclear Engineering
Knoxville, TN 37916
Attn: J. B. Fussell

Woods Hole Oceanographic Institution
Woods Hole, MA 02543
Attn: C. D. Hollister

Environmental Evaluation Group
320 East March Street
P. O. Box 968
Sante Fe, NM 87583
Attn: R. Holland

Chalmers University of Technology
Goteborg
Sweden
Attn: Jan Rydberg

GSF - Institut fur Tieflagerung
Wissenschaftliche Abteilung
D-3392 Clausthal-Zellerfeld
Berliner Strasse 2
West Germany
Attn: L. Dole

Duetsche Gesselschaft fur Wiederaufarbeitung
von Kernbrennstoffen mbH
Bunteweg 2, 3000 Hannover 71
West Germany
Attn: D. R. Proske

Hitachi Shipbuilding and Engineering Co., Ltd.
Plant and Machinery Design Office
3-40 Sakurajina 1-Chome
Konoshana-Ku
Osada, SS4, Japan
Attn: A. Onodera

DISTRIBUTION (cont'd):

Theoretical Physics Division
Building 8.9
AERE Harwell, Oxfordshire
OX 11 ORA
England
Attn: D. Hodgkinson

Nuclear Chemistry and Reactor Division
Hahn-Meitner-Institut fur Kunforschung - Berlin
D-1000 Berline - 39
Glienecken Strasse 100
West Germany
Attn: H. W. Levi

OECD Nuclear Energy Agency
38 Boulevard Suchet
75016 Paris
France
Attn: F. Gera

Boite Postable No. 48
92260 Fontenay-Aux Roses
France
Attn: P. Pages

Studsvik Energiteknik AB
Reactor Systems and Nuclear Safety
S-6111 82 KYKOPING
Sweden
Attn: L. Devell

Royal Institute of Technology
Dept. Land Improvement and Drainage
S-10044 Stockholm 70
Sweden
Attn: R. Thunik

Physikalisch-technische Bundesanstalt
Bundesallee 100
D-3300 Braunschweig
West Germany
Attn: H. Rothemeyer

Bundesanstalt fur Geowissenschaften und Rohstoffe
Stillweg 2
D-3000 Hannover 51
West Germany
Attn: K. Tietze

Karnbranslesakerhet
Fack
S-102 40 Stockholm 5
Sweden
Attn: T. Papp

DISTRIBUTION (cont'd):

A. J. Soinski
California Energy Commission
Nuclear Assessments Office
1111 Howe Avenue, MS #35
Sacramento, CA 95820

Cathy Fore
Ecological Sciences Information Center
Oak Ridge National Laboratory
PO Box X
Oak Ridge, TN 37830

Stephan Ormonde
Quantum Systems, Inc.
PO Box 8575
Albuquerque, NM 87198

Lyn Gelhar
Department of Geoscience
New Mexico Tech
Socorro, NM 87801

John Buckner
E. I. Dupont
Savannah River Laboratory
Aiken, SC 29801

Donald E. Wood
Rockwell Hanford Operations
202-S Bldg.
200 West Area
PO Box 800
Richland, WA 99352

Larry Rickartsen
Science Applications, Inc.
PO Box 843
Oak Ridge, TN 37830

Dan H. Holland, President
New Millennium Associates
1129 State Street, Suite 32
Santa Barbara, CA 93101

V. K. Barwell
Environmental Research Branch
Atomic Energy of Canada Limited
Research Company
Chalk River, Ontario
Canada KOJ1JO

DISTRIBUTION (cont'd):

Paul Kruger
Department of Civil Engineering
Stanford University
Stanford, CA 94305

Ken Dormuth
Environmental and Safety Branch
Atomic Energy of Canada, LTD
Whiteshell Nuclear Research Establishment
Pinawa, Manitoba
Canada ROE1LO

400	C. Winter
1223	R. L. Iman
4000	A. Narath
4400	A. W. Snyder
4410	D. J. McCloskey
	Attn: J. W. Hickman
	G. B. Varnado
	L. D. Chapman
4413	N. R. Ortiz (5)
4413	D. C. Aldrich
4413	M. S. Y. Chu
4413	R. M. Cranwell
4413	F. A. Donath
4413	N. C. Finley
4413	J. C. Helton
4413	D. E. Longsine (5)
4413	R. E. Pepping
4413	L. T. Ritchie
4443	D. A. Dahlgren
4510	W. D. Weart
4511	G. E. Barr
4514	M. L. Merritt
4514	M. S. Tierney
4530	R. W. Lynch
4536	D. M. Talbert
3141	T. L. Werner (5)
3151	W. L. Garner (3)
3154-3	R. P. Campbell (25)
	for NRC distribution to NTIS
8266	E. A. Aas